Mechanism of charge recombination in meso-structured organic-inorganic hybrid perovskite solar cells: A macroscopic perspective

Wenchao Yang, Yao Yao, and Chang-Qin Wu

Articles you may be interested in

Bifacial Si heterojunction-perovskite organic-inorganic tandem to produce highly efficient (η T * ~ 33%) solar cell
Appl. Phys. Lett. **106**, 243902 (2015); 10.1063/1.4922375

Charge transport and recombination in P3HT:PbS solar cells
J. Appl. Phys. **117**, 095503 (2015); 10.1063/1.4913952

The role of a LiF layer on the performance of poly(3,4-ethylenedioxythiophene):poly(styrenesulfonate)/Si organic-inorganic hybrid solar cells
Appl. Phys. Lett. **104**, 083514 (2014); 10.1063/1.4866968

Efficient organic-inorganic hybrid Schottky solar cell: The role of built-in potential
Appl. Phys. Lett. **102**, 113504 (2013); 10.1063/1.4796112

Organic/inorganic hybrid solar cells with vertically oriented ZnO nanowires
Appl. Phys. Lett. **94**, 173107 (2009); 10.1063/1.3126955

Mechanism of charge recombination in meso-structured organic-inorganic hybrid perovskite solar cells: A macroscopic perspective

Wenchao Yang,[1,2] Yao Yao,[1,2,a)] and Chang-Qin Wu[1,2,b)]

[1]*State Key Laboratory of Surface Physics and Department of Physics, Fudan University, Shanghai 200433, China*
[2]*Collaborative Innovation Center of Advanced Microstructures, Fudan University, Shanghai 200433, China*

In the currently popular organic-inorganic hybrid perovskite solar cells, the slowness of the charge recombination processes is found to be a key factor for contributing to their high efficiencies and high open circuit voltages, but the underlying recombination mechanism remains unclear. In this work, we investigate the bimolecular recombination (BR) and the trap-assisted monomolecular recombination (MR) in meso-structured perovskite solar cells under steady state working condition, and try to reveal their roles on determining the device performance. Some interfacial effects such as the injection barriers at the selective contacts are examined as well. Based on the macroscopic device modeling, the recombination resistance-voltage ($R_{rec}-V$) and the current density-voltage ($J-V$) curves are calculated to characterize the recombination mechanism and describe the device performance, respectively. Through comparison with the impedance spectroscopy extracted R_{rec} data, it is found that under the typical BR reduction factor and deep trap densities observed in experiments, the MR dominates the charge recombination in the low voltage regime, while the BR dominates in the high voltage regime. The short circuit current and the fill factor could be reduced by the significant MR but the open circuit voltage is generally determined by the BR. The different electron injection barriers at the contact can change the BR rate and induce different patterns for the $R_{rec}-V$ characteristics. For the perovskites of increased band gaps, the R_{rec}'s are significantly enhanced, corresponding to the high open circuit voltages. Finally, it is revealed that the reduced effective charge mobility due to the transport in electron and hole transporting material makes the R_{rec} decrease slowly with the increasing voltage, which leads to increased open circuit voltage. © 2015 AIP Publishing LLC. [http://dx.doi.org/10.1063/1.4918722]

I. INTRODUCTION

The pursuit of high-efficiency photovoltaic devices has always been advanced by developments of novel light harvesting materials, as being evidenced by the sequential emergences of the crystalline/amorphous silicon solar cells, the inorganic compound Copper indium gallium selenide (CIGS) solar cells, and the organic polymer/fullerene solar cells. In recent years, numerous first principle[1–5] and experimental works[6–9] revealed that the perovskite-structured organometal halide hybrid materials have excellent optoelectronic properties, which are very beneficial for solar energy conversion. For instance, the perovskites are direct band gap semiconducting materials[2,3] and the gaps can be tuned by changing the composition of different halides elements;[1,2,10] the perovskites have broad optical absorption spectra and high incident photo-to-electron conversion efficiency (IPCE).[11,12] As a result, the efficiency experienced a rapid growth and reached to nearly 20% recently.[13] In addition to the high efficiency, people found that the perovskite solar cells can be fabricated with low temperature solution processing method[14,15] and are of high stability.[11,16] Therefore, they become the most promising photovoltaic devices in the future.

In order to find why the perovskite solar cells are so efficient, the device should be considered as a whole where various electronic processes involving the electron transporting material (ETM), the hole transporting material (HTM), and the electrodes may play certain roles. Marchioro *et al.* proposed seven basic processes in which four of them concerns about the recombination.[17] Using time-resolved techniques, they examined different rates of recombination and pointed out that the charge transfer between the perovskite absorption layer and the ETM/HTM is about 1×10^6 times faster than the respective interfacial recombination processes. As is known, less charge recombination implies the higher device efficiency and the larger open circuit voltage. Therefore, this work highlighted the importance of studying the recombination mechanism as well as other electronic processes in perovskite solar cells to understand the macroscopic device behaviors. For this purpose, the device modeling is a suitable theoretical tool.

The early works on charge recombination in perovskite solar cells concerned about the recombination lifetime in the TiO$_2$ electron transporting network or in different HTM's.[18–20] Then, the transient photoluminescence (PL) is employed to study the recombination kinetics in the pristine perovskite,[21,22] which elucidated the roles of bimolecular and monomolecular recombination (MR) mechanisms under different excitation intensities. However, for meso-structured

a)yaoyao@fudan.edu.cn
b)cqw@fudan.edu.cn

perovskite solar cells, the ETM and HTM also participate and thus complicate the transport and the recombination processes, and their roles must be taken into account. Moreover, since the recombination mechanism in the steady state current condition may not be necessarily equivalent to that in the transient condition, the recombination mechanism needs to be investigated by taking advantage of the information from the steady state measurements to make our understanding of this problem more relevant to the real working devices. Recently, people intensively employed the recombination resistance (R_{rec}) data extracted from the impedance spectroscopy (IS)[23] to characterize the recombination processes for different device setups and working conditions.[15,24–27] The R_{rec}–V diagrams were plotted and found to exhibit different patterns. Since the R_{rec} is inversely proportional to the recombination rate R, while the applied voltage is a direct measure of the internal charge carrier density n, these patterns may provide important information on the order of recombination α ($R \propto n^{\alpha}$) and need further interpretation from a theoretical point of view.

In this paper, we use the device model method to simulate the current density-voltage (J–V) and the R_{rec}–V characteristics of meso-structured perovskite solar cells. The calculated R_{rec}–V curves are compared with the IS extracted ones to reveal the recombination mechanism inside the photoactive layer. It is found that the reduced bimolecular recombination (BR) and the Shockley-Read-Hall (SRH) MR both play important roles in the devices, but each one dominates the recombination mechanism in different voltage regimes. The results are consistent with the experimental findings of photoluminescence and photoconductance.[21,28] The paper is organized as follows. In Sec. II, the device structures and the device model adapted to the perovskite context are described. In Sec. III, we present the simulation results based on the BR and the MR mechanisms and investigate the influences of the contact injection barriers, the BR reduction factor, the increased band gaps, and the effective mobility reduction effect, which are found to be able to influence the patterns of the R_{rec}–V curves, and thus the device performance. In Sec. IV, we draw the conclusions.

II. THEORETICAL MODELING OF PEROVSKITE SOLAR CELLS

A meso-structured perovskite solar cell, as illustrated in Fig. 1(a), basically consists of the following layers: the glass substrate, the fluorine-doped transparent oxide (FTO) anode, the compact TiO$_2$ layer, the photoactive perovskite layer, the HTM (like spiro-OMeTAD) capping layer, and the heavy metal cathode such as gold. The perovskite is spin-coated on the mesoporous metal oxides scaffold such as TiO$_2$ or Al$_2$O$_3$, where TiO$_2$ also acts as ETM, while Al$_2$O$_3$ does not.[12] The HTM layer is covered on the perovskite layer with some HTM being infiltrated into the mesoporous scaffold to facilitate charge separation and the extraction of holes. Although the meso-structured perovskite solar cells inherit lots of features from the traditional solid state dye-sensitized solar cells, they also have some common features with the organic bulk heterojunction solar cells in terms of
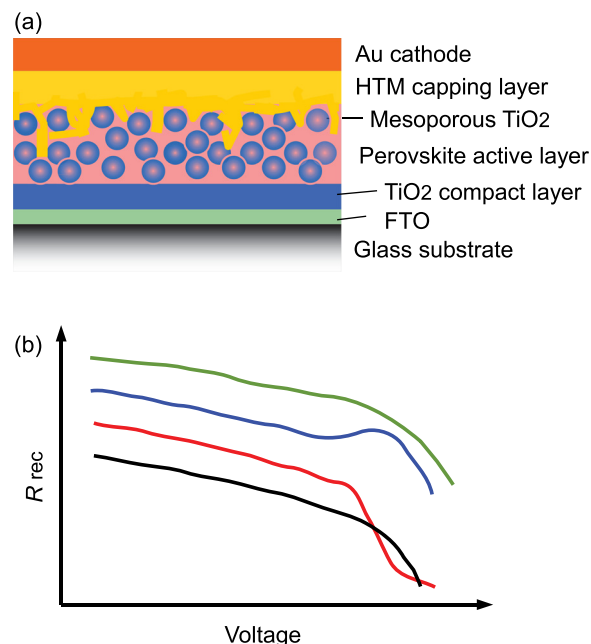

FIG. 1. The schematic illustrations for the cross-sectional structure of a NS perovskite solar cell (a) and the four typical patterns of the recombination resistance R_{rec} versus the applied bias voltage V (b).[26] The R_{rec}–V characteristics are generally extracted from the impedance spectroscopy measurement combined with an equivalent circuit model.[24] Notice that all the lines in (b) are just intended to illustrate the experimental patterns rather than represent their relative magnitudes.

the structure, given to the similar roles played by the perovskite/ETM(HTM) interfaces in the former and the donor/acceptor interfaces in the latter. Therefore, the method for simulating the inorganic or organic solar cells,[29,30] i.e., the macroscopic device model can be well adapted for modeling the meso-structured perovskite solar cells. In their recent work, Minemoto *et al.* demonstrated the application of device model to the planar heterojunction perovskite solar cells.[31]

In this model, the photoactive layer, which is actually the composite of the perovskite, the ETM and the HTM, is considered as an effective medium of homogeneous property. On its left and right boundaries lie the TiO$_2$ compact layer and the spiro-OMeTAD capping layer, respectively, which form electron and hole selective contacts.[25] Compared with the respective electronic processes in planar heterojunction solar cells, the charge separation is facilitated by the ETM and HTM, but the charge recombination could occur either in the perovskite itself or on the perovskite/ETM(HTM) interfaces.[17] Moreover, for most of their lifetimes in the photoactive layer the free charge carriers are transported in the ETM and the HTM rather than in the perovskite, since in the meso-structured device architecture the electrons and holes do not have to travel far before reaching an interface so that the charge transfer processes are almost instant (with a timescale of picosecond[32]). These complications can be circumvented by inserting proper parameters into the model. Given to the small electron (hole) mobility and the charge trapping effect in the TiO$_2$ (spiro-OMeTAD),[18,19] we intentionally employed effective electron/hole mobilities which are smaller than the mobilities in the pristine perovskite by 1 or 2 orders of magnitude, in order to

characterize such kind of transport property in meso-structured perovskite solar cells. On the contrary, in planar heterojunction solar cells such an effect is absent. In Subsection III E, we discuss elaborately the influence of the effective mobility reduction due to the slow charge transport in the ETM and the HTM, and compare it to the case in planar heterojunction solar cells.

Currently, it is generally accepted that in the perovskite the exciton binding energy is very low and the primary optical excitation is free charge carriers.[33,34] However, the exciton concept is still extensively used, and the coexistence of free carriers and excitons may give a proper description to the real situation,[22,28,35] which can cover both extreme cases. Therefore, we first write down the equation for exciton dynamics

$$\frac{\partial X}{\partial t} = D_X \frac{\partial^2 X}{\partial x^2} - \frac{X}{\tau} - k_{cs}X + G(x), \qquad (1)$$

where X is the exciton density. On the right hand side of Eq. (1), the first term stands for the exciton diffusion with a diffusivity D; the second term accounts for the radiative and nonradiative recombination of excitons with a recombination lifetime of τ; the third term represents the exciton dissociation at the perovskite/ETM and perovskite/HTM interfaces, with k_{cs} the common charge separation rate.[17] Since the exciton binding energy is comparable or much smaller to the thermal energy of 26 meV under the room temperature 300 K, the exciton dissociation can spontaneously take place in a timescale of picoseconds and the charge transfer to the ETM or HTM usually occurs in a sub-picosecond time scale.[32,34] Thus, the k_{cs} should be sufficiently high. $G(x)$ is the exciton generation rate due to light absorption and of the form

$$G(x) = G_0 \exp(-x/L_a), \qquad (2)$$

with L_a the light absorption length.

Secondly, the continuity equations for holes and electrons generated by exciton dissociation are written as

$$\frac{\partial p}{\partial t} = -\frac{1}{e}\frac{\partial J_p}{\partial x} + k_{cs}X - r(x), \qquad (3)$$

$$\frac{\partial n}{\partial t} = \frac{1}{e}\frac{\partial J_n}{\partial x} + k_{cs}X - r(x), \qquad (4)$$

where p and n are hole and electron density, respectively, and the electron(hole) current density has the drift-diffusion form

$$J_{n(p)}(x) = e\mu_{n(p)}\left(n(p)E \pm \frac{kT}{e}\frac{\partial n(p)}{\partial x}\right), \qquad (5)$$

in which the Einstein's relation $D_{n(p)} = \mu_{n(p)}kT/e$ has been assumed.

The recombination rate $r(x)$ in Eqs. (3) and (4) contains both the MR rate and the BR rate. The MR rate r_m is calculated according to the SRH trap-assisted recombination process

$$r_m = \frac{C_n C_p N_t (np - n_i^2)}{C_n(n + n_1) + C_p(p + p_1)}. \qquad (6)$$

Here, $C_n(C_p)$ denotes the capture coefficient for electrons (holes) being captured by the deep sub-gap trap states, and N_t is the trap level density. n_1, p_1 are the equilibrium density of trapped electrons and holes, which obey $n_1 p_1 = n_i^2$ with n_i the intrinsic carrier density. Throughout this work, we assume the depth of deep traps is 0.5 eV lower than the conduction band edge. The BR rate accounts for the direct recombination between the electrons in the conduction band and the holes in the valence band, and is written as

$$r_b = \gamma(np - n_i^2), \qquad (7)$$

where the Langevin prefactor $\gamma = e(\mu_n + \mu_p)/\varepsilon_0\varepsilon$. Thus, the total recombination rate reads

$$r(x) = r_m + r_b. \qquad (8)$$

Finally, the time evolution of the internal electric field is governed by the spatial-integrated Poisson's equation[36]

$$\frac{\partial E}{\partial t} = -\frac{1}{\varepsilon_0\varepsilon}\left(J(x) - \frac{1}{L}\int_0^L J(x)dx\right) - \frac{1}{L}\frac{\partial V(L,t)}{\partial t}, \qquad (9)$$

where $V(L, t)$ is the externally applied bias voltage and the left boundary electric potential $V(0, t)$ is set to 0.

Equations (1), (4), (3), and (9) can be solved to obtain the steady state solutions after proper boundary conditions are imposed to them. First, since no exciton can escape from the active layer, the exciton current at each boundary equals to zero

$$\left.\frac{\partial X}{\partial x}\right|_{x=0} = \left.\frac{\partial X}{\partial x}\right|_{x=L} = 0. \qquad (10)$$

Moreover, at the left boundary, under equilibrium there is a detailed balance between the extracted electron current and the back-transferred electron current. After light absorption or dark charge injection, this balance is broken and the interfacial electron current density reads

$$J_n(0) = eS_n(n(0) - n_0), \qquad (11)$$

in which S_n is the extraction or surface recombination velocity of the electrons. Here, we set it to be AT^2/eN_c with A the Richardson's constant and N_c the density of states of the perovskite conduction band. $n_0 = N_c \exp(-\phi_n/kT)$ is the equilibrium electron density at the left contact. ϕ_n is the energy level offset between the compact TiO$_2$ and the perovskite, or the electron injection barrier at the contact. Following the same argument, the expression

$$J_p(L) = eS_p(p(L) - p_0) \qquad (12)$$

holds for the hole current on the right boundary. Because the compact TiO$_2$ and the spiro-OMeTAD both form selective contacts with the photoactive layer,[25] no surface electron (hole) current exists on the right (left) boundary, and we have

TABLE I. The parameters for device modeling.

Name	Symbol	Values
Band gap[1,2]	E_g	1.55 eV
Exciton lifetime	τ	100 ns
Effective electron/hole mobility	μ_n, μ_p	1×10^{-5} m^2/Vs
Exciton generation rate	G_0	1.2×10^{28} m^{-3} s^{-1}
Optical absorption length	L_a	100 nm
Free carrier generation rate	k_{cs}	1 nm^{-3} s^{-1}
Dielectric constant[3]	ϵ	20
Room temperature thermal energy	kT	26 meV
Thickness of the photoactive layer	d	300 nm
DOS of the conduction/valence band	N_c, N_v	10^{27} m^{-3}

$$J_n(L) = J_p(0) = 0. \tag{13}$$

In the actual simulations, for the perovskite the simulation parameters, which are listed in Table I, are based on the measurements or the first principle calculations to the most frequently used methylammonium (MA) lead triiodine (MAPbI$_3$). For instance, considering the charge transport in ETM and HTM, the effective electron/hole mobilities for the composite of MAPbI$_3$ (which is ambipolar material), meso-porous TiO$_2$, and spiro-OMeTAD are set to be 10^{-5} m^2/Vs. The exciton generation rate G_0 is set to be a high value given to the high IPCE of the perovskite under 1 sun illumination. The free charge generation rate k_{cs} is the thermal-activated exciton dissociation rate or the interfacial charge transfer rate, and we find that 1 ns^{-1} is a sufficiently high value for the simulation purpose, since under this value the calculated J–V curves are actually indistinguishable with the free carrier J–V curves. The other relevant parameters will be noted in the respective subsections.

III. RESULTS AND DISCUSSION

Generally, the IS extracted R_{rec}–V plots exhibit four typical kinds of patterns,[24–26] as illustrated in Fig. 1(b). With increasing applied voltage, all the R_{rec}'s experience a slow decreasing in the low voltage regime and a much faster decreasing in the high voltage regime. However, some of them also exhibit additional features: the red line has a "high voltage tail" at the vicinity of the open circuit voltage; the

blue line has an obvious kink; and the green line's "high voltage decreasing part" is not so steep as the corresponding part on the black line. To reveal the recombination mechanism suggested by these patterns, it is helpful to reproduce them through the device model calculation under different working conditions. Theoretically, the R_{rec} is defined as[24]

$$R_{rec} = \frac{1}{A} \left(\frac{\partial J_{rec}}{\partial V} \right)^{-1}, \tag{14}$$

where A is the area of the device surface and the recombination current density

$$J_{rec} = e \int_0^L r(x) dx. \tag{15}$$

According to the definition, R_{rec} plays the role of a shunt resistance. The larger the R_{rec}, the better the device performance.

A. The role of the bimolecular recombination and the impact of charge injection barriers at the contacts

To investigate the roles of BR and MR mechanisms independently, we first focus on the BR mechanism and take only the BR rate into account in the device model. Simultaneously, the effect of the Schottky contact at the electrode/perovskite interface is also examined by varying the injection barriers in the simulation, since these barriers due to the interfacial energy level offset may be different and are found to be essential for achieving high efficiency perovskite solar cells.[13] For simplicity, the hole barrier ϕ_p is fixed to be 0.2 eV (corresponding to the hole contact of spiro-OMeTAD), while the electron barrier ϕ_n is varied among the values of 0.2 eV, 0.4 eV, and 0.5 eV. The cases of ϕ_n being equal to 0.2 eV and 0.4 eV may both correspond to the compact TiO$_2$ electron contact, and the 0.5 eV case can represent the ITO electron contact in the inverted device structure.[37] The simulated J–V and R_{rec}–V curves are shown in Fig. 2 and the obtained device operating parameters are listed in Table II.

In Fig. 2(a), it can be observed that all the J–V curves show large fill factors of over 60%, which arise from the
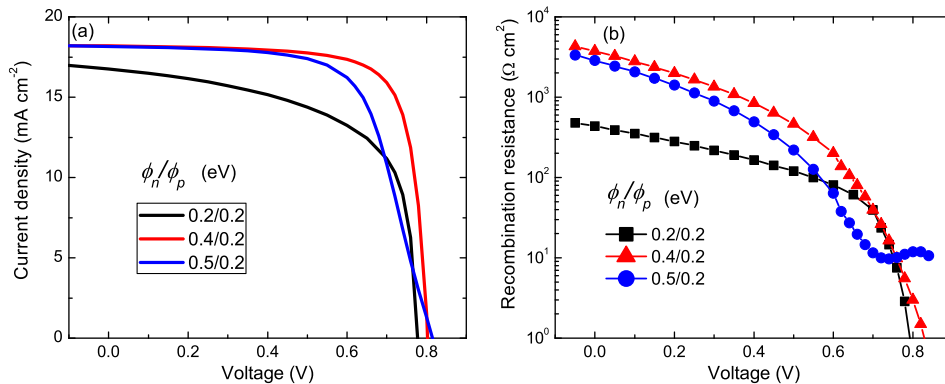

FIG. 2. The current density-voltage (J–V) characteristics (a) and the R_{rec}–V characteristics (b) for different electron injection barrier ϕ_n and a fixed hole injection barrier ϕ_p of 0.2 eV. Only the bimolecular recombination term (Eq. (7)) is taken into account in the calculations. The different electron injection barriers may correspond to different electron selective contacts, such as a compact TiO$_2$ layer or a PCBM layer. The simulation parameters are as stated in Sec. II.

TABLE II. The device working parameters calculated for a set of charge injection barriers.

ϕ_n, ϕ_p	J_{sc} (mA/cm^2)	V_{oc} (V)	FF (%)
0.2,0.2	16.76	0.78	63.5
0.4,0.2	18.19	0.80	76.6
0.5,0.2	18.16	0.82	65.4

high balanced mobilities of the perovskite photoactive layer. The short circuit current density J_{sc} s and the open circuit voltage V_{oc} s both differ among the curves, in which the 0.4 eV curve presents the largest J_{sc} s of 18.2 mA/cm^2, while the 0.5 eV curve exhibits the slightly larger V_{oc} of 0.82 V than the others. The distinctive effects induced by different injection barriers can be observed more clearly on the R_{rec}–V characteristics, as shown in Fig. 2(b). With increasing voltage, all the R_{rec}'s first experience a relative slow decreasing in the reversed or low voltage regime and then a very rapid one when approaching the V_{oc}. Therefore, this decreasing behavior of R_{rec} with voltage, just as illustrated by the black line in Fig. 1, may be the characteristic feature of the BR mechanism. In the low voltage regime, the R_{rec} of 0.2 eV is of the smallest value and thus leads to the smallest J_{sc}. This is because in this case the dark injected electrons accumulate near the contact, which recombine with the optically generated holes through radiative BR and make the recombination rate increase. For Schottky contacts with larger injection barriers, this interfacial electron accumulation is negligible so that the R_{rec} increases to some extent (the 0.4 eV case). However, the large injection barrier also plays the role of a series resistance, on which a substantial proportion of the built-in voltage fall so that the charge carriers cannot be swept out efficiently due to the weak internal electric field. Consequently, for $\phi_n = 0.5$ eV the R_{rec} in the low voltage regime decreases to the decreased J_{sc} and fill factor. As to the open circuit voltage, it is closely related to the behavior of the R_{rec} in the high voltage regime. For the 0.5 eV case, the R_{rec} decreases much slower wherein and becomes larger than the others when the voltage exceeds 0.7 V, and the maximum V_{oc} of 0.82 V is also achieved accordingly. Moreover, in this case there appears the "high voltage tail" on the R_{rec}–V curve as illustrated by the red line in Fig. 1. This characteristic pattern is also originated from the high injection barrier or the contact resistance. The interfacial electric field due to the voltage fall on this Schottky contact resistance depletes the electrons nearby and reduces the total recombination rate.

Compared with the R_{rec}–V curves obtained experimentally through the IS combined with an equivalent circuit model, our calculated results exhibit the similar order of magnitude (10^3 Ω cm^2) and give the approximate decreasing behavior with increasing bias voltage. This suggests that the Langevin type BR must be a recombination mechanism in perovskite solar cells under steady state working condition, and play important roles on determining the device performance. This finding is consistent with the experimental results of the transient photoluminescence and the time-resolved microwave conductivity (TRMC),[21,28] except that a proper

BR reduction factor ζ is not incorporated, which will be addressed in Subsection III C. Because the fill factors of the experimental J–V curves are not as large as 80%, the results with ϕ_n being equal to 0.5 eV may more or less provide a good approximation to the real situation. Thus, we will fix ϕ_n to 0.5 eV for the calculations afterward.

B. The role of the SRH monomolecular recombination

There have been many first principle calculations for the electronic states induced by the intrinsic defects.[38–40] It is found that the most of the intrinsic defects only create shallow traps, which is also verified by the TRMC experiment.[41] Nevertheless, the same calculations revealed some types of intrinsic defects indeed create deep trap levels lying near the center of the band gap, such as the Pb interstitial, I vacancy and I-on-MA anti-site in MAPbI$_3$.[40] While the shallow sub-gap levels have slight influence on the material transport and recombination properties, these deep trap levels may lead to significant trap assisted SRH recombination. In addition, it is reported that the organic cation MA$^+$ may form hole traps and the Pb^{2+} cation can be both electron and hole traps.[42] Thus, it is insightful to consider the roles of the SRH recombination on the overall recombination mechanism and device performance. It can be demonstrated from Eq. (6) that the effective MR lifetime τ_{mr} is inversely proportional to the product of the capture coefficient C_p, C_n and the trap density N_t. Without loss of generality, we fix C_p and C_n to the same value and change N_t to vary τ_m in the actual calculations. Then in the device model, the $r(x)$ is the summation of the BR rate r_b and the MR rate r_m. The calculated J–V and R_{rec}–V curves for a set of deep trap density are shown in Fig. 3.

It can be observed that if the trap density N_t is equal to or below 5×10^{22} m^{-3} (corresponding to a τ_m of about 100 ns), the J–V and R_{rec}–V curves only deviate from the respective trap free ones in the low voltage regime. When N_t reaches 5×10^{23} m^{-3}, the J–V curve exhibits the obviously reduced J_{sc} and fill factor but the V_{oc} remains unchanged. Correspondingly, the R_{rec} decreases to some extent in the low voltage regime, but a kink appears when the applied voltage is greater than 0.6 V, leading to a delayed decreasing of the R_{rec}. Therefore, MR only affects the device performance around the short circuit condition. As the applied voltage increases, the charge carrier density increases accordingly, and the trap levels are gradually filled so that they cannot act as recombination centers. In this case, the BR mechanism overwhelms the MR mechanism and determines the value of V_{oc}. This is analogous to the charge carrier recombination behavior in the polymer/fullerene bulk heterojunction (BHJ) solar cells.[43]

When N_t is of an extremely large (and unrealistic) value of 5×10^{24} m^{-3} ($\tau_m \simeq 1$ ns), the J–V curve is greatly deformed and shows rather small J_{rec} and fill factor, suggesting huge recombination losses. The increased MR rate not only induces a significant reduction for R_{rec} but also changes the overall pattern of the R_{rec}–V curve, on which a kink at 0.6 V can be clearly observed. On the left side of this kink, the R_{rec} is almost invariant as the applied voltage, which is a
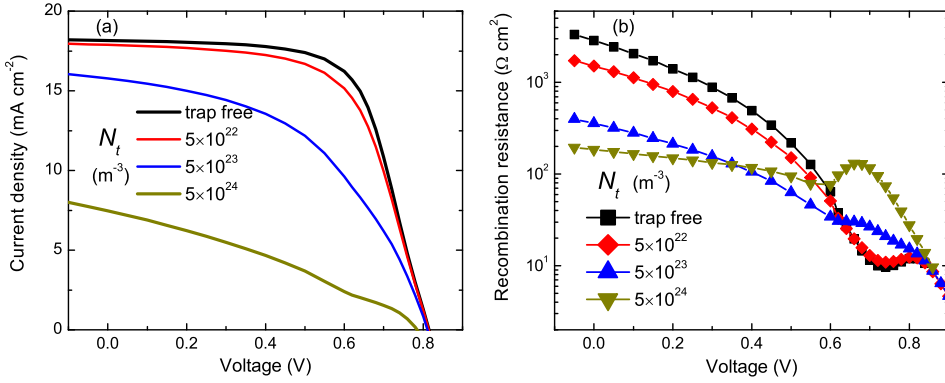
FIG. 3. The J–V curves and the R_{rec}–V characteristics calculated with both BR and MR processes being taken into account. The MR rate R_{mr} takes the form of the Shockley-Read-Hall (SRH) Eq. (6), in which the electron/hole capture coefficient C_p and C_n are both fixed to be 2×10^{-16} m^3/s, while the trap density N_t is varied for several orders of magnitude. The depth of the traps is assumed to be 0.5 eV below the LUMO level.

signature of the MR dominated recombination mechanism; while on the right side of the kink, the BR mechanism overwhelms the MR mechanism and leads to rapid reduction of R_{rec} and a relatively small V_{oc} of 0.78 V. This is because under the high applied voltage, the huge number of injected dark carriers may fill some deep trap levels and enhance the charge carrier density, and thus significantly contribute to the BR rate r_b. In our case, the dark carriers are mainly holes becomes of the low ϕ_p of 0.2 eV, and the calculated hole density is enhanced by 3 orders of magnitude with the increasing of the voltage from 0 V to 0.78 V. Referring to Fig. 1(b), it can be deduced that the relatively flat (the blue curve) pattern may arise from high deep trap density and thus the high MR rate in the low voltage regime. The kink therein is exactly the transition region between the two types of recombination mechanisms.

Therefore, if the deep trap density is extremely large, the SRH MR will be significant in the low voltage regime, which induces the reduction of J_{sc} and the fill factor but has minor influence on the V_{oc}. When the open circuit condition is achieved, the BR dominates the recombination mechanism, and the V_{oc} is still basically determined by it. Stranks *et al.* studied the pristine perovskite with the photoluminescence experiment and claimed that the MR is the dominant recombination mechanism under 1 sun illumination, while BR only dominates under much higher illumination intensities.[22] This is because in the PL experiment the electrodes are absent and there is no dark injected carriers in the photoactive layer. Thus under the open circuit condition, the charge carrier density therein is diminished relative to the full devices so that the r_b is probably underestimated. Besides, the reduced BR effect is found to prevail in the perovskites and needs to be incorporated into the device model, which can strongly influence the relative importance of the MR mechanisms over the BR mechanism. This effect will be discussed in Subsection III C.

C. The role of reduced bimolecular recombination

Recently, many experimental and first principle works revealed that the reduced BR effect also exists in the perovskite solar cells.[28,32,35,41] However, unlike the cases of organic solar cells where the main underlying reason lies on the different electron properties between the donors and acceptors, such as the mobilities and dielectric constants, the reduced BR is more likely an intrinsic feature of the perovskite material itself.[28,35] Furthermore, if we consider the roles of the ETM and HTM in the photoactive layer, the processes of ultrafast interfacial charge transfer upon photoexcitation in the perovskite, and the extremely slow back-transfer into the perovskite make the electrons (holes) be transported solely in ETM (HTM), so that the two types of carriers are spatially well separated, which also reduces the BR rate.[17] Whatever the microscopic mechanism of reduced BR, here we focus on the macroscopic impacts of this effect and investigate the variation of the R_{rec}–V characteristics and the device performance under this situation.

We take into account the reduced BR in simulation by multiplying the ordinary r_b with a reduction factor ζ, which represents the ratio between the actual BR rate and that given by the Langevin's theory

$$r_b = \zeta\gamma(np - n_i^2). \tag{16}$$

A deep trap density of 5×10^{22} m^{-3} is also employed in the calculations. The calculated J–V and R–V curves are shown in Fig. 4. From Fig. 4(a), it is found that the most obvious effect of incorporating the ζ is the increasing of V_{oc} compared to that without (the black solid line). This increasing can be understood from general V_{oc} expression in terms of charge carrier density

$$V_{oc} = \frac{E_g}{e} - \frac{kT}{e}\ln\left(\frac{N_c N_v}{np}\right)$$
$$= \frac{E_g}{e} - \frac{kT}{e}\ln\left(\frac{\zeta\gamma N_c N_v}{G_c}\right), \tag{17}$$

where G_c is the charge carrier generation rate under the open circuit condition. Equation (17) is valid as long as MR is absent or negligible (corresponding to $\zeta = 1$, 0.1). In this case, V_{oc} increases by 0.04 V as ζ decreases by one order of magnitude. On the other hand, for $\zeta = 0.01$ the V_{oc} is 0.89 V, and that for $\zeta = 0.001$ does not increase any more.

Correspondingly, as shown in Fig. 4(b), as the ζ begins to decrease from 1 to 0.1, the R_{rec} is enhanced to some extent, because the R_{rec} is inversely proportional to the total rate $r(x)$. However, for smaller ζ the weight of r_m increases in the total rate $r(x)$, and the enhancement of R_{rec} becomes marginal. The R_{rec}–V curve for $\zeta = 0.01$ even coincides with that for $\zeta = 0.001$. This is because of the moderately large N_t assumed in the calculation, under such small ζ the MR rate r_m becomes comparable to the reduced BR rate r_b (Eq. (16))
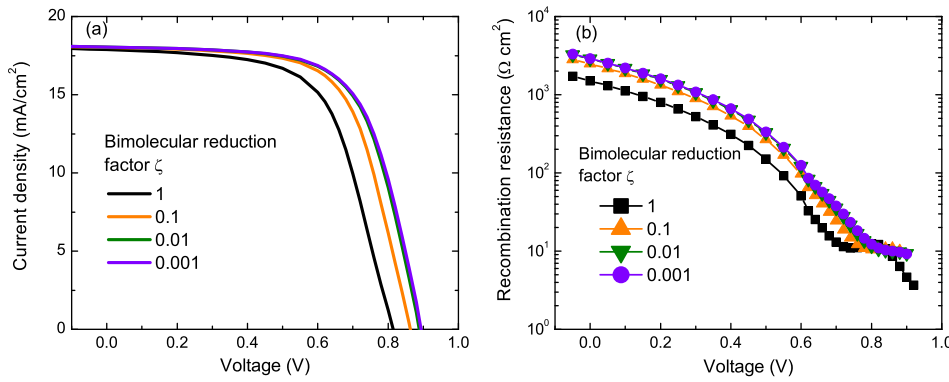
FIG. 4. The J–V curves (a) and the R_{rec}–V characteristics (b) under different BR reduction factor ζ's. The MR is also taken into account in the simulation, and the deep trap density is fixed to be $5 \times 10^{22}\,\mathrm{m}^{-3}$. The V_{oc}'s corresponding to the J–V curves with increasing ζ are 0.82 V, 0.86 V, 0.89 V, and 0.9 V, respectively.

and thus forms an important loss pathway, which suppress the further increasing of R_{rec} and the V_{oc}. It is the combined effects of the BR and MR mechanisms that determine the overall device performance.

In Fig. 5, we plotted the J–V and R_{rec}–V curves for the fixed ζ of 0.001 and a set of deep trap densities. It can be observed that the R_{rec} decreases significantly as the N_t increases by one order of magnitude. Accordingly, the obtained values of J_{sc}, V_{oc}, and fill factor are all very sensitive to the given value of N_t and experience drastic losses with the increased N_t. This is in strong contrast to the case of $\zeta = 1$ (shown in Fig. 3), in which the loss is only significant for extremely large N_t's. Moreover, notice that for the trap free case, the calculated R_{rec} is in the order of $10^6\ \Omega\,\mathrm{cm}^2$, which far exceeds the experimentally obtained ones (in the order of $10^4\ \Omega\,\mathrm{cm}^2$ or below) and is too large to be realistic. This provides an important evidence for the existence of MR in a working meso-structured perovskite solar cell. In addition, the characteristic kinks also appear on the curves R_{rec} with the large N_t. All these facts manifest the important roles played by the MR mechanism for its rate is comparable to the BR rate under such small ζ. Thus in order to improve the device performance, the intrinsic defects or the deep traps must be controlled under low levels so that the loss induced by MR mechanism can be suppressed as much as possible.

D. The impact of increased band gap due to the mixed halide composition

In the perovskite structure MAPbX$_3$, X can be the halide elements of I, Cl, Br, or their mixture. It is found that by changing the proportion of different halide elements the band gap of the resulting perovskite material can be tuned

continuously from 1.55 eV (100% I) to 2.3 eV (100% Br). Utilizing this effect, people can fabricate tandem solar cells which are able to efficiently harvest photons in a wide spectrum. Suarez et al. measured the R_{rec}–V characteristics for the meso-structured perovskite solar cells with some typical mixed halide compositions.[26] They found that the R_{rec}'s increases with increasing of the Cl or Br ratio with respect to I. This suggests the total recombination rate decreases with increasing of the material band gap. To reveal the underlying reason of this effect, we calculate the J–V and the R_{rec}–V curves for three band gap values, in which 1.55 eV corresponds to MAPbI$_3$, 2.3 eV to MAPbBr$_3$, and 1.7 eV represents a composition between the two cases. Even though the absorbance for materials of different band gaps is certainly different, in the calculation we used the same optical generation rate to focus on the electronic processes and compare the device efficiency under the same density level for the optically generated free charge carriers. The deep trap density is still fixed to $5 \times 10^{22}\,\mathrm{m}^{-3}$. The results are shown in Fig. 6.

For the calculated J–V curves, as can be expected, the J_{sc} and the fill factor remain invariant, but the V_{oc} increases drastically. In particular, for 2.3 eV the calculated V_{oc} is about 1.5 V, just being a little bit larger than the experimentally acquired maximum value of 1.3 V under the same chemical composition.[44] As to the variation of R_{rec}, from Fig. 6(b) it is found that the larger the band gap, the higher the R_{rec}, which could be understood as follows. Because the band gap E_g corresponds to a built-in voltage of $V_{bi} = E_g - \phi_n - \phi_p$, the increased E_g gives rise to the increased V_{bi} and thus a decreased charge carrier extraction time $t_{tr} = L^2 / \mu_{n(p)} (V_{bi} - V)$ (V is the applied voltage). In this
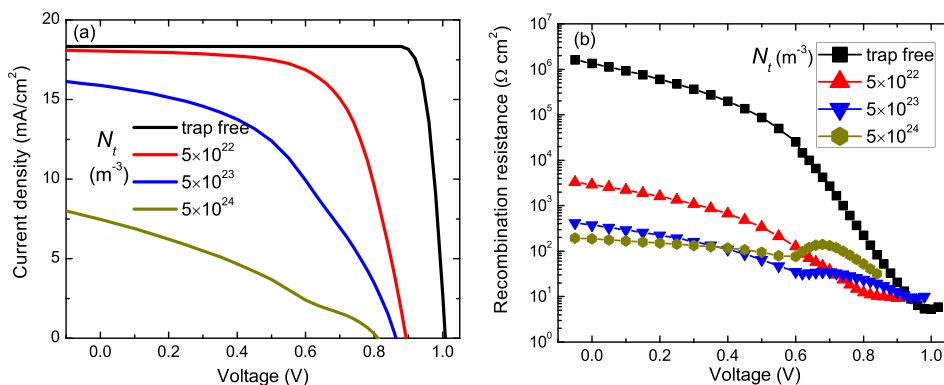

FIG. 5. The J–V curves (a) and the R_{rec}–V characteristics (b) under different deep trap densities. The BR reduction factor ζ is fixed to 0.001. The MR is also taken into account in the simulation, and the deep trap density is fixed to be $5 \times 10^{22}\,\mathrm{m}^{-3}$. The calculated V_{oc}'s corresponding to the J–V curves with increasing trap density are 1 V, 0.9 V, 0.86 V, and 0.82 V, respectively.

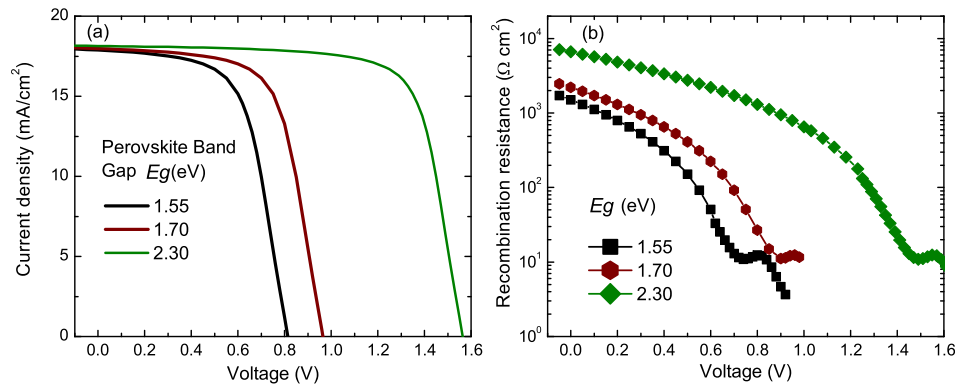FIG. 6. The simulated J–V curves (a) and the R_{rec}–V characteristics (b) for different band gaps of perovskite structure photoactive materials MAPbX3 with different halide (X) composition. The 1.55 eV case corresponds to the MAPbI3 and the 2.3 eV case to the MAPbBr3, while the 1.7 eV case is of a mixed halide composition. Both the BR and MR are taken into account in the simulation, and the trap density is fixed to be 5×10^{22} m^{-3}. The V_{oc}s corresponding to the three calculated J−V curves are 0.82 V, 0.96 V, and 1.57 V, respectively.

case, the charge carriers have less chances of colliding with each other and recombine together through BR mechanism, leading to a reduced BR rate and the high R_{rec}. Furthermore, for 2.3 eV, the decreasing behavior of R_{rec} with increasing voltage looks not so steep as the others, since with increase V_{bi} the efficient extraction of charge carriers can be maintained for a broader voltage range, in which the recombination rate does not increase rapidly with applied voltage. This delayed increasing of the recombination rate also leads to the high V_{oc}. The kind of "slow decreasing" pattern can also be found in the IS extracted R_{rec}–V curves (the green line in Fig. 1(b)).

E. The impact of the effective mobility reduction due to the charge transport in the ETM/HTM

The MAPbX$_3$ perovskite materials are ambipolar materials which have high mobilities for both electrons and holes.[32,35] However, in meso-structured perovskite solar cells, following the charge separation process the free electrons and holes are transported in ETM (TiO$_2$ scaffold) and HTM (spiro-OMeTAD) respectively, before being extracted by the two electrodes. It is found that in the meso-structured perovskite solar cells the electron transport process is restricted by its diffusion inside in the TiO$_2$ mesoporous particles.[19] Moreover, a recent TRMC experiment revealed that for the spiro-OMeTAD/perovskite/TiO$_2$ system, the TRMC signal ($\phi \sum \mu_{max}$, which directly corresponds to the total mobility) is significantly suppressed compared to that in the pristine perovskite or the perovskite/TiO$_2$ systems,[41] suggesting the mobility of charge carriers in meso-structured perovskite solar cells may be greatly reduced. Because the BR prefactor γ contains the sum of electron and hole mobilities, the reduced mobility will also change the charge recombination mechanism and consequently affect the device efficiency. In our device model, considering the difference between the charge carrier mobility in the perovskite and that in the ETM/HTM, we had assumed an effective electron (hole) mobility for the transporting of electrons (holes) in the meso-structured photoactive layer of homogeneous property. The effective mobilities are about 1 order of magnitude lower than the mobility in the pristine perovskite. In order to

examine the impact of the effective mobility reduction effect on device performance, we calculate the J–V and the R_{rec}–V characteristics for two effective mobilities that differ by 1 order of magnitude, in which the larger value of 1×10^{-4} m^2/Vs corresponds to a pristine perovskite photoactive layer and thus the planar heterojunction perovskite solar cells.

In Fig. 7(a), the J–V curves for both different effective mobility $\mu_{n,p}$ and the BR reduction factor ζ are plotted. Here, we concentrate on the $\zeta = 0.01$ cases, since the existence of ζ has been experimentally verified; and for $\zeta = 1$, the curves show similar behaviors. Compared with the low effective mobility case, we find that the high mobility case gives rise to a lower V_{oc} but a higher fill factor. The variation of V_{oc} can still be understood from Eq. (17) where the γ is reduced under the small effective mobilities. The R_{rec}–V curves are plotted in Fig. 7(b). It can be observed that the value of R_{rec} for the high $\mu_{n,p}$ decreases rapidly with the increasing applied voltage. Even though the R_{rec} for $\mu_{n,p} = 10^{-4}$ m^2/Vs is 1 order of magnitude larger than that for $\mu_{n,p} = 10^{-5}$ m^2/Vs in low voltage regime (which arises from the efficient charge extraction near the short circuit condition), the latter decreases rather slowly and retains a larger value of about 10 Ω cm^2 when approaching the open circuit condition, leading to a larger V_{oc} in that case. Thus, it can be concluded that the slow decreasing R_{rec} on the IS extracted R_{rec}–V plots may be due to the inefficient charge transport in ETM or HTM.

Furthermore, Fig. 7(b) shows the different behavior of the R_{rec} in the planar heterojunction devices and the meso-structured devices. In the planar heterojunction devices, the photoactive layer is the pristine perovskite and the electron/hole mobilities are sufficiently high, the R_{rec}–V curves reveal that the ζ can greatly enhance the R_{rec}, and thus significantly improve the J_{sc}, V_{oc}, and the fill factor.[45] On the other hand, in the meso-structured devices, the R_{rec} is only moderately increased as a result of the small *zeta*, and it is not sensitively dependent on the applied voltage. The pattern exhibited by the curve for $\zeta = 0.01$, $\mu_{n,p} = 10^{-5}$ m^2/Vs can best mimic the experimentally extracted R_{rec}−V pattern (the red curve in Fig. 1(b)) in meso-structured perovskite solar cells. Therefore, without the knowledge of the actual effective
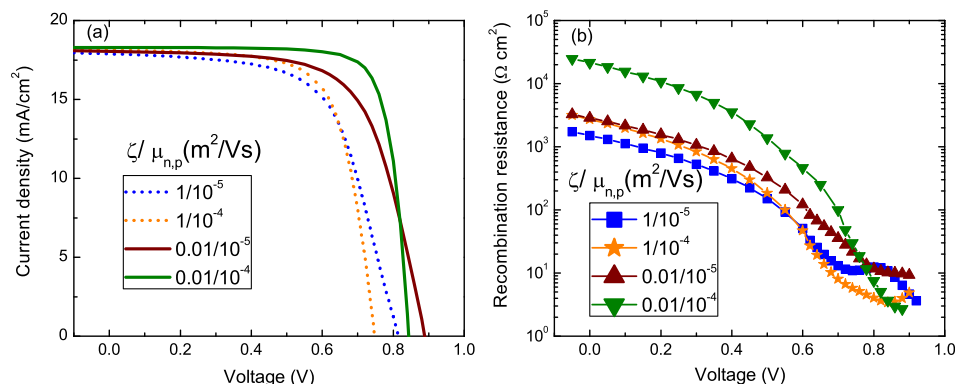
FIG. 7. The simulated J–V curves (a) and R_{rec}–V characteristics (b) under the different electron/hole effective mobilities (balanced) and the BR reduction factor ζs. The trap density used in the simulation is still 5×10^{22} m^{-3}. The cases for $\mu_{n,p} = 10^{-4}$ m^2/V s correspond to pristine perovskite photoactive layers, which represent the planar heterojunction devices; while the cases for $\mu_{n,p} = 10^{-5}$ m^2/V s correspond to meso-structured photoactive layers, which represent the meso-structured devices.

mobilities, in previous simulations we employ the value of 5×10^{-5} m^2/Vs to take into account this mobility reduction effect.

IV. CONCLUSION

To find the steady state charge recombination mechanism in meso-structured perovskite solar cells, we employed a device model containing the basic electronic processes in the perovskite photoactive layer to simulate the J–V and R_{rec}–V characteristics under the working conditions. We show that by solely employing the Langevin type BR rate the calculated R_{rec} is comparable to the IS extracted ones in terms of the order of magnitude and the decreasing behavior with increasing voltage, suggesting the BR is an important recombination mechanism in the working perovskite solar cells. For large trap density, the MR mechanism induces the decreasing of R_{rec} in the low voltage regime, which damages the J_{sc} and the fill factor, but the V_{oc} is basically determined by the BR mechanism. After taking into account the BR reduction effect generally observed in perovskite materials, the MR mechanism becomes important for small reduction factor ζ and the enhancement of R_{rec} is suppressed by the MR mechanism if the trap density is just moderately large. This fact along with the experimentally observed order of magnitude of the ζ and the R_{rec} provides the existence for the importance of MR mechanism in the perovskite. Generally, MR dominates the recombination in the low voltage regime, while BR dominates in the high voltage regime. As to the characteristic patterns of the R_{rec}–V curves, the "high voltage tail" is found to be induced by the Schottky contact and the "kink" is identified with the transition between the BR and the MR mechanisms. For the mixed halide perovskite materials of large band gaps, the R_{rec}'s are enhanced due to the increased built-in field, which results in efficient charge extraction and smaller recombination rate. The impacts of the mobility reduction due to the electron (hole) transport in ETM (HTM) are also investigated. With reduced effective mobility, the R_{rec} decreases slowly and becomes less voltage dependent than that in the pristine perovskite, which corresponds to the case of planar heterojunction solar cells.

[1]E. Mosconi, A. Amat, M. K. Nazeeruddin, M. Graetzel, and F. D. Angelis, J. Phys. Chem. C **117**, 13902 (2013).
[2]J. Even, L. Pedesseau, J. M. Jancu, and C. Katan, J. Phys. Chem. Lett. **4**, 2999 (2013).
[3]F. Brivio, A. B. Walker, and A. Walsh, APL Mater. **1**, 042111 (2013).
[4]Y. Wang, T. Gould, J. F. Dobson, H. Zhang, H. Yang, X. Yao, and H. Zhao, Phys. Chem. Chem. Phys. **16**, 1424 (2014).
[5]A. Filippetti and A. Mattoni, Phys. Rev. B **89**, 125203 (2014).
[6]D. B. Mitzi, J. Chem. Soc. Dalton Trans. **2001**, 1.
[7]T. Baikie, Y. Fang, J. M. Kadro, M. Schreyer, F. Wei, S. G. Mhaisalkar, M. Graetzel, and T. J. White, J. Mater. Chem. A **1**, 5628 (2013).
[8]C. C. Stoumpos, C. D. Malliakas, and M. G. Kanatzidis, Inorg. Chem. **52**, 9019 (2013).
[9]H. J. Snaith, J. Phys. Chem. Lett. **4**, 3623 (2013), also see the references therein.
[10]J. H. Noh, S. H. Im, J. H. Heo, T. N. Mandal, and S. I. Seok, Nano Lett. **13**, 1764 (2013).
[11]H. S. Kim, C. R. Lee, J. H. Im, K. B. Lee, T. Moehl, A. Marchioro, S. J. Moon, R. H. Baker, J. H. Yum, J. E. Moser, M. Graetzel, and N. G. Park, Sci. Rep. **2**, 591 (2012).
[12]M. M. Lee, J. Teuscher, T. Miyasaka, T. N. Murakami, and H. J. Snaith, Science **338**, 643 (2012).
[13]H. Zhou, Q. Chen, G. Li, S. Luo, T. Song, H. S. Duan, Z. Hong, J. You, Y. Liu, and Y. Yang, Science **345**, 542 (2014).
[14]J. Burschka, N. Pellet, S. J. Moon, R. H. Baker, P. Gao, M. K. Nazeeruddin, and M. Graetzel, Nature **499**, 316 (2013).
[15]J. T. W. Wang, J. M. Ball, E. M. Barea, A. Abate, J. A. A. Webber, J. Huang, M. Saliba, I. M. Sero, J. Bisquert, H. J. Snaith, and R. J. Nicholas, Nano Lett. **14**, 724 (2014).
[16]A. Mei, X. Li, L. Liu, Z. Ku, T. Liu, Y. Rong, M. Xu, M. Hu, J. Chen, Y. Yang, M. Graetzel, and H. Han, Science **345**, 295 (2014).
[17]A. Marchioro, J. Teuscher, D. Friedrich, M. Kunst, R. W. D. Krol, T. Moehl, M. Graetzel, and J. E. Moser, Nat. Photonics **8**, 250 (2014).
[18]Y. Zhao and K. Zhu, J. Phys. Chem. Lett. **4**, 2880 (2013).
[19]Y. Zhao, A. M. Nardes, and K. Zhu, J. Phys. Chem. Lett. **5**, 490 (2014).
[20]D. Bi, L. Yang, G. Boschloo, A. Hagfeldt, and E. M. J. Johansson, J. Phys. Chem. Lett. **4**, 1532 (2013).
[21]Y. Yamada, T. Nakamura, M. Endo, A. Wakamiya, and Y. Kanemitsu, J. Am. Chem. Soc. **136**, 11610 (2014).

[22]S. D. Stranks, V. M. Burlakov, T. Leijtens, J. M. Ball, A. Goriely, and H. J. Snaith, Phys. Rev. Appl. **2**, 034007 (2014).

[23]J. R. Jennings, Y. Liu, F. S. Alamuti, and Q. Wang, J. Phys. Chem. C **116**, 1556 (2012).

[24]V. G. Pedro, E. J. J. Perez, W. S. Arsyad, E. M. Barea, F. F. Santiago, I. M. Sero, and J. Bisquert, Nano Lett. **14**, 888 (2014).

[25]E. J. J. Perez, M. Wußler, F. F. Santiago, K. L. Wollny, E. Mankel, T. Mayer, W. Jaegermann, and I. M. Sero, J. Phys. Chem. Lett. **5**, 680 (2014).

[26]B. Suarez, V. G. Pedro, T. S. Ripolles, R. S. Sanchez, L. Otero, and I. M. Sero, J. Phys. Chem. Lett. **5**, 1628 (2014).

[27]A. Dualeh, T. Moehl, N. Tetreault, J. Teuscher, P. Gao, M. Nazeeruddin, and M. Graetzel, ACS Nano **8**, 362 (2014).

[28]T. J. Savenije, C. S. Ponseca, L. Kunneman, M. Abdellah, K. Zheng, Y. Tian, Q. Zhu, S. E. C. I. G. Scheblykin, T. Pullerits, A. Yartsev, and V. Sundström, J. Phys. Chem. Lett. **5**, 2189 (2014).

[29]R. Sokel and R. C. Hughes, J. Appl. Phys. **53**, 7414 (1982).

[30]L. J. A. Koster, E. C. P. Smits, V. D. Mihailetchi, and P. W. M. Blom, Phys. Rev. B **72**, 085205 (2005).

[31]T. Minemoto and M. Murata, J. Appl. Phys. **116**, 054505 (2014).

[32]C. S. Ponseca, T. J. Savenije, M. Abdellah, K. Zheng, A. Yartsev, T. Pascher, T. Harlang, P. Chabera, T. Pullerits, A. Stepanov, J. P. Wolf, and V. Sundstrom, J. Am. Chem. Soc. **136**, 5189 (2014).

[33]Q. Lin, A. Armin, R. C. R. Nagiri, P. L. Burn, and P. Meredith, Nat. Photonics **9**, 106 (2014).

[34]J. S. Manser and P. V. Kamat, Nat. Photonics **8**, 737 (2014).

[35]C. Wehrenfennig, G. E. Eperon, M. B. Johnston, H. J. Snaith, and L. M. Herz, Adv. Mater. **26**, 1584 (2014).

[36]P. S. Davids, I. H. Campbell, and D. L. Smith, J. Appl. Phys. **82**, 6319 (1997).

[37]R. Lindblad, D. Bi, B. W. Park, J. Oscarsson, M. Gorgoi, H. Siegbahn, M. Odelius, E. M. J. Johansson, and H. Rensmo, J. Phys. Chem. Lett. **5**, 648 (2014).

[38]W. J. Yin, T. Shi, and Y. Yan, Appl. Phys. Lett. **104**, 063903 (2014).

[39]W. J. Yin, T. Shi, and Y. Yan, Adv. Mater. **26**, 4653 (2014).

[40]M. L. Agiorgousis, Y. Y. Sun, H. Zeng, and S. Zhang, J. Am. Chem. Soc. **136**, 14570 (2014).

[41]H. Oga, A. Saeki, Y. Ogomi, S. Hayase, and S. Seki, J. Am. Chem. Soc. **136**, 13818 (2014).

[42]I. A. Shkrob and T. W. Marin, J. Phys. Chem. Lett. **5**, 1066 (2014).

[43]S. R. Cowan, A. Roy, and A. J. Heeger, Phys. Rev. B **82**, 245207 (2010).

[44]E. Edri, S. Kirmayer, D. Cahen, and G. Hodes, J. Phys. Chem. Lett. **4**, 897 (2013).

[45]W. Yang, Y. Yao, and C. Q. Wu, J. Appl. Phys. **117**, 095502 (2015).